Energy dependence of exact muffin-tin-orbital structure constants

A. E. Kissavos,[1] L. Vitos,[2,3,4] and I. A. Abrikosov[1]
[1]*Department of Physics, Chemistry and Biology, University of Linköping, SE-581 83 Linköping, Sweden*
[2]*Applied Materials Physics, Department of Materials Science and Engineering, Royal Institute of Technology, SE-10044, Stockholm, Sweden*
[3]*Condensed Matter Theory Group, Physics Department, Uppsala University, S-75121 Uppsala, Box 530, Sweden*
[4]*Research Institute for Solid State Physics and Optics, P.O. Box 49, H-1525 Budapest, Hungary*
(Received 31 October 2006; published 15 March 2007)

We investigate the energy dependence of the exact muffin-tin-orbital slope matrix in the complex energy plane. Analytic expressions for the asymptotic behavior of the slope matrix and its first energy derivative for large imaginary energies are given. We demonstrate that a two-center Taylor type expansion of the slope matrix accurately reproduces the exact values within a complex energy range covering the usual energy window used in electronic structure calculations. As an application, we study the composition dependence of the lattice parameters of the MgY binary system, a candidate material for hydrogen storage applications.

DOI: 10.1103/PhysRevB.75.115117 PACS number(s): 71.15.Ap, 71.15.Dx, 71.20.Be, 61.66.Dk

I. INTRODUCTION

The effort to separate in an electronic structure problem the information about the crystal structure from the information about the particular atoms which compose the material, can be traced back to the structure and form factors of pseudopotential theory.[1–3] Splitting the problem into potential and structure dependent parts makes this approach conceptually clean and efficient, since the structural dependent part can be calculated once and for all for each crystal structure. One of the most elegant ways to achieve this is offered by the multiple scattering problem formulated within the Korringa-Kohn-Rostoker (KKR) method.[4,5] In this approach, the structural information is accumulated in the energy dependent structure constant matrix and the electronic structure is calculated using the Green's function formalism.

In the 1970s, Andersen and co-workers introduced the linear muffin-tin-orbital (LMTO) method.[6–10] The KKR and LMTO methods were shown[11] to be closely related within the atomic sphere approximation.[6,12] However, the latter method provided an alternative way to gain more knowledge about the KKR approach, and, due to the energy linearization, it could be applied to systems containing up to ~100 atoms per unit cell. In early 1980s, it was realized that the bare LMTO structure constants could be transformed into screened or tight-binding (TB) structure constants.[13] Because of this, it became possible to calculate the LMTO structure constants in real space and formulate efficient order-N methods for both bulk[14,15] and surface[16,17] systems. Later, it turned out that the long-range bare KKR structure constants could also be screened in a similar fashion as the TB-LMTO structure constants, which led to the development of the screened KKR method.[18–21]

In most of the applications of the above methods, calculations were carried out within nonoverlapping muffin-tin or atomic sphere approximations for the one-electron potential. The recently developed exact muffin-tin-orbital (EMTO) theory[22] offered a possibility to go beyond these approximations and properly describe the interstitial region in the case of overlapping muffin-tin wells. In this formalism, the screening is realized using infinity high potential spheres centered on lattice sites. The degree of localization of the EMTO structure constants is determined by the radii of these nonoverlapping hard spheres.[22] The EMTO method[23–25] combined with the full charge density (FCD) technique[26] has proven to produce results in close agreement with those obtained using formally exact but very cumbersome full-potential methods.[25,27–30] As with the KKR, the EMTO method also uses the Green's function technique to solve the multiple scattering problem. This makes the EMTO suitable for treating the disordered alloys within the coherent potential approximation (CPA).[31,32] The accuracy of the EMTO-CPA method[33] has been demonstrated in the case of binary and multicomponent random alloys.[33–39]

During a self-consistent calculation, the structure constant matrix has to be computed for complex energies. For instance, due to the Green's function formalism, integrations involving the density of states are performed in the complex energy plane.[40] In EMTO method, this is carried out on a circular or elliptic contour enclosing the valence states below the Fermi level ϵ_F. Moreover, in theories going beyond the traditional local density approximation, e.g., the dynamical mean field theory (DMFT),[41–43] the many-body problem is solved on a linear contour $z=\epsilon_F+i\omega_n$, where ω_n are the Matsubara frequencies. Usually, the maximum frequency included is around 2-5 times the bandwidth,[44] which for metals is typically $\sim 0.5-1.0$ Ry. Therefore, there is a clear demand for knowledge about the nature of the structure constants and how they behave in the complex energy plane. The main purpose of this work is to explore this question in the case of the EMTO method. A related problem is how the energy dependence of the structure constants and their energy derivatives can be described within the energy window of interest. Here, we derive an efficient and accurate parametrization and discuss the consequences of our finding.

In this paper, we will keep the original name and refer to the EMTO structure constant matrix as the slope matrix.[22] In Sec. II, we briefly review the theory behind the EMTO basis sets, the EMTO slope matrix, and the screening transformations connecting the EMTO slope matrix to the KKR structure constant matrix. In this Section, two different param-

etrized formulas are given. In Sec. III, we show how the slope matrix and its first energy derivative behave in the complex energy plane, and establish analytical expressions valid for large imaginary energies. Here we also discuss the accuracy of the proposed energy parametrizations and demonstrated them in the case of hcp La. The two-center expansion is applied in Sec. IV, where we investigate the variation of the lattice parameters of Mg-rich MgY alloy. The paper ends with conclusions.

II. THE EMTO SLOPE MATRIX

In a muffin-tin (MT) method, the effective one-electron potential $v(\mathbf{r})$ is approximated by the muffin-tin potential $v_{MT}(\mathbf{r})$, viz.

$$v(\mathbf{r}) \approx v_{MT}(\mathbf{r}) \equiv v_0 + \sum_R [v_R(r_R) - v_0], \tag{1}$$

where R runs over the lattice sites, and $\mathbf{r}_R \equiv r_R \hat{r}_R = \mathbf{r} - \mathbf{R}$. The spherical potentials $v_R(r_R)$ become equal to v_0 outside the potential spheres of radii s_R. For nonoverlapping potential wells, $v_R(r_R)$ reduces to the spherical part of $v(\mathbf{r})$ around site R and v_0 to the conventional muffin-tin zero. However, in the EMTO method large overlaps between muffin-tin spheres are allowed. It has been demonstrated[23,45] that the accuracy of the MT approximation can be improved substantially by increasing the overlap between the potential spheres. In this case, the spherical symmetric potentials are chosen in a way that, together with the parameter v_0, to give the best approximation to the effective one-electron potential. Minimizing the mean of the squared deviation between the left and the right hand side of Eq. (1) leads to a set of integral or differential equations for $v_R(r_R)$ and v_0. For further details about the optimized overlapping muffin-tin potentials the reader is referred to Refs. 23 and 45.

According to the MT approximation, the trial one-electron wave function can be expanded in terms of the usual partial waves inside the potential spheres and wave-equation solutions outside the spheres. When the linear combination of these local solutions are joined continuously or differentiable at the spheres boundary, the obtained wave function will be a solution for the Schrödinger equation in all space.

A. The basis sets

In the EMTO formalism, outside the potential spheres the basis set is formed by the screened spherical waves $\Psi^a_{RL}(\kappa^2, \mathbf{r}_R)$. They are defined as the solutions of the Helmholtz wave equation

$$[\nabla^2 + \kappa^2]\Psi^a_{RL}(\kappa^2, \mathbf{r}_R) = 0 \tag{2}$$

in conjunction with boundary conditions set at nonoverlapping hard spheres with radii $a_{R'l'}$ centered at lattice site R'. Here $\kappa^2 = \epsilon - v_0$, ϵ is the energy, and L is an abbreviation for the combined angular momenta $L \equiv \{lm\}$. The screened spherical waves form a complete basis set in the a interstitial. They behave as a pure real harmonic $Y_L(\hat{r}_R)$ on their own a spheres, while the $Y_{L'}(\hat{r}_{R'})$ projections on all the other a spheres vanish. With these energy independent boundary conditions, for κ^2 below the bottom of the a spheres continuum, the screened spherical waves have short range and weak energy dependence.

The $\Psi^a_{\mathrm{RL}}(\kappa^2, \mathbf{r}_R)$ function centered on site R may be expanded in terms of real harmonics $Y_{L'}(\hat{r}_{R'})$ around any site R' as

$$\Psi^a_{RL}(\kappa^2, \mathbf{r}_R) = f^a_{Rl}(\kappa^2, r_R) Y_L(\hat{r}_R) \delta_{RR'} \delta_{LL'} + \sum_{L'} g^a_{Rl}(\kappa^2, r_{R'}) Y_{L'}(\hat{r}_{R'}) S^a_{R'L'RL}(\kappa^2). \tag{3}$$

Here the expansion coefficients $S^a_{R'L'RL}(\kappa^2)$ are the elements of the EMTO slope matrix. The two radial functions f and g can be expressed in terms of Bessel $j_l(\kappa^2, r)$ and Neumann $n_l(\kappa^2, r)$ functions[46] as follows:

$$\begin{aligned} f^a_{Rl}(\kappa^2, r) &= {}^1t_{Rl} n_l(\kappa^2, r) + {}^2t_{Rl} j_l(\kappa^2, r), \\ g^a_{Rl}(\kappa^2, r) &= -{}^3t_{Rl} n_l(\kappa^2, r) - {}^4t_{Rl} j_l(\kappa^2, r), \end{aligned} \tag{4}$$

where the t_{Rl} are the elements of the screening matrix defined by

$$\begin{pmatrix} {}^1t_{Rl}(\kappa^2) & {}^2t_{Rl}(\kappa^2) \\ {}^3t_{Rl}(\kappa^2) & {}^4t_{Rl}(\kappa^2) \end{pmatrix} = 2\frac{a^2_{Rl}}{w} \begin{pmatrix} \dfrac{\partial j_l(\kappa^2, a_{Rl})}{\partial r_R} & -\dfrac{\partial n_l(\kappa^2, a_{Rl})}{\partial r_R} \\ \dfrac{1}{a_{Rl}} j_l(\kappa^2, a_{Rl}) & -\dfrac{1}{a_{Rl}} n_l(\kappa^2, a_{Rl}) \end{pmatrix}, \tag{5}$$

and w is the average atomic radius. Finally, from the matching condition formulated at the potential and hard spheres one arrives to the kink cancellation equation

$$\sum_{RL} a_{R'} [S^a_{R'L'RL}(\kappa^2) - \delta_{R'R}\delta_{L'L} D^a_{Rl}(\epsilon)] v^a_{RL}(\epsilon) = 0, \tag{6}$$

where $D^a_{Rl}(\epsilon)$ is the logarithmic derivative function calculated at the a_{Rl} sphere and $v^a_{RL}(\epsilon)$ are the expansion coefficients for the trial wave function. This equation yields the one-electron energies and wave vectors. The number of states is computed using the overlap matrix expressed in terms of the first order energy derivative of the slope matrix and of the logarithmic derivative function. More details about the EMTO formalism can be found in Refs. 22–25 and 33.

B. Calculation of the slope matrix

The EMTO slope matrix can be obtained from the bare KKR structure constant matrix $S^0_{R'L'RL}(\kappa^2)$ as[22]

$$S^a_{R'L',RL}(\kappa^2) = \frac{{}^1t_{Rl}}{{}^3t_{Rl}} \delta_{R'R}\delta_{L'L} - \frac{1}{{}^3t_{R'l'}} \left[-S^0(\kappa) - \frac{{}^4t_{Rl}}{{}^3t_{Rl}} \right]^{-1}_{R'L'RL} \frac{2a_{Rl}}{w^3 {}^3t_{Rl}}. \tag{7}$$

The bare structure constants are defined as

$$S^0_{R'L'RL}(\kappa^2) = -8\pi \sum_{L''} C_{LL'L''} \frac{(2l''-1)!!}{(2l'-1)!!(2l-1)!!} \times [-(\kappa w)^2]^{(l'+l-l'')/2} (-1)^l n_{L''}(\kappa, \mathbf{R}' - \mathbf{R}), \tag{8}$$

where $C_{LL'L''}$ are the real Gaunt numbers. In order to express the energy derivatives of the slope matrix, we introduce the dimensionless energy parameter $\omega \equiv (\kappa w)^2$. After rearranging Eq. (7), we get

$$\sum_{R''L''} \mathcal{B}_{R'L'R''L''}(\omega) A_{R''L''RL}(\omega) = -2\frac{a_R}{w} \delta_{R'R} \delta_{L'L}, \tag{9}$$

where we have introduced the notations

$$\mathcal{A}_{R'L'RL}(\omega) \equiv \frac{{}^1t_{Rl}(\omega)}{{}^3t_{Rl}(\omega)} \delta_{R'R} \delta_{L'L} - S^a_{R'L'RL}(\omega) \tag{10}$$

and

$$\mathcal{B}_{R'L'RL}(\omega) \equiv {}^3t_{R'l'}(\omega) [{}^4t_{Rl}(\omega) \delta_{R'R} \delta_{L'L} + S^0_{R'L'RL}(\omega) {}^3t_{Rl}(\omega)]. \tag{11}$$

The screening parameters, likewise the slope matrix, depend on energy through ω.[22,25] Applying the product rule, from (9) we obtain the j-th energy derivative of the slope matrix as

$$\frac{d^j S^a(\omega)}{d\omega^j} = B(\omega)^{-1} \left[\sum_{i=0}^{j-1} \frac{j!}{(j-i)!i!} \frac{d^{j-i}\mathcal{B}(\omega)}{d\omega^{j-i}} \frac{d^i \mathcal{A}(\omega)}{d\omega^i} + 2\frac{a}{w}\delta_{j,0} \right] + \frac{d^j}{d\omega^j} \frac{{}^1t(\omega)}{{}^3t(\omega)}, \tag{12}$$

where the RL subscripts have been dropped and the matrix multiplication is implied. The energy derivatives of the bare structure constant $S^0(\omega)$ are calculated directly from Eq. (8). The derivatives of the screening parameters are obtained from the energy derivatives of the Bessel and Neumann functions.

When the slope matrix is calculated on the real energy axis, one prefers to use as basis functions the Bessel and Neumann functions for positive ω and Bessel and Hankel functions for negative ω. In this case the slope matrix will be real on the real energy axis. If one needs to calculate the slope matrix for a general complex energy, it is more convenient to use everywhere the Bessel and Hankel functions. In this case, the slope matrix is complex everywhere except for negative real energies.

C. Parametrization of the slope matrix

For a self-consistent calculation, the slope matrix is required within an energy window that includes energies between the bottom of the valence band ϵ_b and the Fermi level ϵ_F plus ~0.2 Ry above the Fermi level. In systems with deep laying core states and a narrow valence band structure, we can take $\epsilon_F - \epsilon_b \approx 1.4$ Ry. Since $\epsilon_F - v_0$ is typically around ~0.6 Ry, for such systems the slope matrix should be calculated approximately for $-0.8\ \text{Ry} \leqslant \omega/w^2 \leqslant 0.8$ Ry. Using an average $w^2 = 10\ \text{Bohr}^2$, the energy interval of interest in terms of ω turns out to be ± 8 around $\omega = 0$. For these energies, the slope matrix may be approximated by an n-th order Taylor expansion[23,25] written around ω_0, viz.

$$S^a(\omega) \approx S^a_n(\omega;\omega_0) \equiv S^a(\omega_0) + \frac{1}{1!}\frac{dS^a(\omega)}{d\omega}(\omega-\omega_0) + \frac{1}{2!}\frac{d^2S^a(\omega)}{d\omega^2}(\omega-\omega_0)^2 + \cdots + \frac{1}{n!}\frac{d^nS^a(\omega)}{d\omega^n}(\omega-\omega_0)^n. \tag{13}$$

The energy derivatives are obtained using the analytic expression (12). In practice, the expansion center ω_0 is chosen somewhere close to 0 and $n=6$.

In a system with large characteristic bandwidth, problems may occur in the numerical determination of the slope matrix from the expansion (13). First, for v_0 lying far below the Fermi energy, i.e., for $\epsilon_F - v_0 \sim 1.0$ Ry or larger, expression (13) diverges for energies near and above ϵ_F. The second problem arises for bands, where $\epsilon_b \ll v_0$. Then Eq. (13) breaks down for energies near the bottom of the valence band. In such systems, the semicore states are located with a few Ry below the Fermi level. A typical energy window for these elements is approximately 2–3 Ry below v_0 and 1 Ry above v_0. Both of the above problems become more pronounced in solids with large w.

The most straightforward way to improve the behavior of the expansion for a large energy window is to include a second expansion around a large negative ω. Due to the contour integration, joining the two expression may lead to large errors. To overcome them and assure a reasonable high accuracy, the energy integral should be performed separately on an upper and a lower energy contour enclosing the valence and the semicore states, respectively. However, in alloys and compounds where the band gap between the valence and semicore states contains other states, using different energy panels is not feasible.

Alternatively, we may introduce additional screening spheres in the system. This is done by inserting extra screening spheres E in the interstitial positions in addition to the original screened spheres A located on the lattice sites. In this way, one improves on the localization of the screened spherical waves, and reduces the interstitial region, and thus the characteristic size of the system. To keep the original representation for the potential, we use vanishing potential spheres on the E sites. By this procedure, the energy window, where expansion (13) converges, can be increased significantly.[47] Using the Löwdin technique, it is easy to show[47] that the kink cancellation equation (6), written for the $A+E$ system, reduces to the original problem written only for the A spheres. However, in order to avoid the above discussed convergence problems near the energies far from v_0, one should always use the $A+E$ equation rather than the A equation. This is because the screening is improved due to the extra hard spheres and as a consequence the energy derivatives of the slope matrix are computed with higher numerical accuracy than those for the parent lattice. The main

drawback of the $A+E$ technique is the increased computational time.

The above approach indicates that the convergence of the expansion (13) could be improved by increasing the accuracy used in the numerical determination of the high order energy derivatives and possibly by include more terms in the expansion, i.e., using $n>6$. In principle, the energy derivatives can be computed directly from Eq. (12), but in order to maintain the accuracy with increasing j, one must then also increase the size of the real space cluster used to solve the Dyson equation (7).[48] However, the number of surface resonances, due to the finite size of the cluster,[22] also increases with the surface area. Another way to generate accurate high order derivatives is to use data calculated for different energies. This can be formulated as a two-center expansion. Here we consider only the two-center expansion, but of course the technique can be generalized for an arbitrary number of expansion centers. We consider two distinct energy points ω_1 and ω_2 where the value and derivatives of S^a are known. We expand $S^a(\omega)$ in such a way that the expansion should reproduce exactly the first n derivatives of S^a in ω_1 and the value and the first m derivatives of S^a in ω_2. Mathematically, this can be formulated as

$$S^a(\omega) \approx S^a_{n,m}(\omega;\omega_1,\omega_2) = S^a_n(\omega;\omega_1) + \frac{1}{(n+1)!}a_{n+1}(\omega-\omega_1)^{n+1} + \cdots + \frac{1}{(n+m)!}a_{n+m+1}(\omega-\omega_1)^{n+m+1}, \tag{14}$$

where $S^a_n(\omega;\omega_1)$ is defined in Eq. (13). The $(m+1)$ coefficients a_{n+i} are obtained from the $(m+1)$ conditions

$$S^a_{n,m}(\omega_2;\omega_1,\omega_2) = S^a(\omega_2),$$

$$\left.\frac{dS^a_{n,m}(\omega;\omega_1,\omega_2)}{d\omega}\right|_{\omega=\omega_2} = \left.\frac{dS^a(\omega)}{d\omega}\right|_{\omega=\omega_2}, \ldots$$

$$\left.\frac{d^m S^a_{n,m}(\omega;\omega_1,\omega_2)}{d\omega^m}\right|_{\omega=\omega_2} = \left.\frac{d^m S^a(\omega)}{d\omega^m}\right|_{\omega=\omega_2}. \tag{15}$$

These conditions lead to a system of linear equations for $a_{n+1}, a_{n+2}, \ldots, a_{n+m+1}$. Solving these equations we obtain $S^a_{n,m}(\omega;\omega_1,\omega_2)$, which is in fact an $(n+m+1)$-th order expansion for $S^a(\omega)$ around ω_1.

III. RESULTS

A. Energy dependence of the slope matrix

To investigate the energy dependence of the EMTO slope matrix, we consider the face centered cubic (fcc) lattice. The fcc slope matrix has been calculated using *spd* basis set and a real space cluster of 79 lattice vectors. After performing the Bloch summation, we focus on the *ss* ($L=L'=\{0,0\}$) diagonal element of $S^a_{LL'}(\kappa^2)$ and its first energy derivative calculated in the center of the Brillouin zone. The reason for using in this test only the *ss* sub-blocks is that these are the largest and the most delocalized ones within the real space. These two functions are plotted in Fig. 1 in terms of energy for an interval corresponding to the dimensionless parameter ω with real part $[x=\mathrm{Re}(\omega)]$ between -10 and $+10$ and imaginary part $[y=\mathrm{Im}(\omega)]$ between 0 and 10. Since $\mathrm{Im}[S^a(x+iy)]=-\mathrm{Im}[S^a(x-iy)]$, valid for the first energy derivative as well, results are shown only for positive $\mathrm{Im}(\omega)$.

Along the real axis, the real part of the slope matrix, shown in the panel (a) of Fig. 1, follows the trend already discussed in Ref. 25. In the complex plane, $\mathrm{Re}(S^a)$ decreases with the imaginary energy component for any $\mathrm{Re}(\omega)$. Panel (b) shows the imaginary part of the slope matrix. This is zero on the negative real axis and very small along the positive real axis. On the other hand, $\mathrm{Im}(S^a)$ rises rapidly as one goes out into the complex plane.

In panels (c) and (d) of Fig. 1, we show the real and imaginary parts of the first energy derivative of the slope matrix. Both of these functions are very small, except for large positive $\mathrm{Re}(\omega)$, where they are already affected by the presence of the poles. As with $\mathrm{Im}(S^a)$, the imaginary part of the energy derivative of the slope matrix is zero or almost zero on the real axis, even if one can see small oscillations around $8-10\omega$. We note that these oscillations are also present in the higher energy derivatives. Hence, except for large positive $\mathrm{Re}(\omega)$, the slope matrix and its first energy derivative exhibit smooth and weak energy dependence, which indicates that accurate parametrization of these functions exist.

Figure 2 shows the behavior of the *ss* sub-block of the slope matrix and its first order energy derivative for $\mathrm{Im}(\omega) \leqslant 50$. Here, the real part of ω was taken to be zero. The trends from Fig. 2 can be understood by looking to the asymptotic behavior of the basis functions. As the imaginary part of the energy increases, the Hankel functions and thus the bare structure constants go exponentially to zero. The screening, however, modifies the energy dependence of the slope matrix, which can easily be seen from Eq. (7). The off-diagonal elements of $S^a_{LL'}$ are found to decay exponentially, just as the bare structure constants, while the diagonal terms behave as

$$S^a_{ll}(\omega) = l - \sqrt{\omega}\frac{h_{l+1}(\omega)}{h_l(\omega)}, \tag{16}$$

where $h_l(\omega)$ is the Hankel function. In the limit of large imaginary values of ω, this expression goes to $(i\sqrt{\omega}-1)$ for any l. That is, $\mathrm{Re}(S^a)\to -\mathrm{Im}(\sqrt{\omega})-1$ and $\mathrm{Im}(S^a)\to \mathrm{Re}(\sqrt{\omega})$ when $\mathrm{Im}(\omega)\to\infty$. Our calculations performed for $\mathrm{Im}(\omega) \gg 50$ (not shown) demonstrate that S^a approaches its asymptotic expression within a few percent for $\mathrm{Im}(\omega) \approx 250-300$. Note that for an average $w^2=10$ Bohr^2, these ω values correspond to 25–30 Ry imaginary energy, which is well beyond the maximum Matsubara frequency included in a DMFT calculation.[41–43] For the energy derivative of the slope matrix, the off-diagonal terms decay exponentially, while the diagonal terms decay as $1/|\sqrt{\omega}|$.

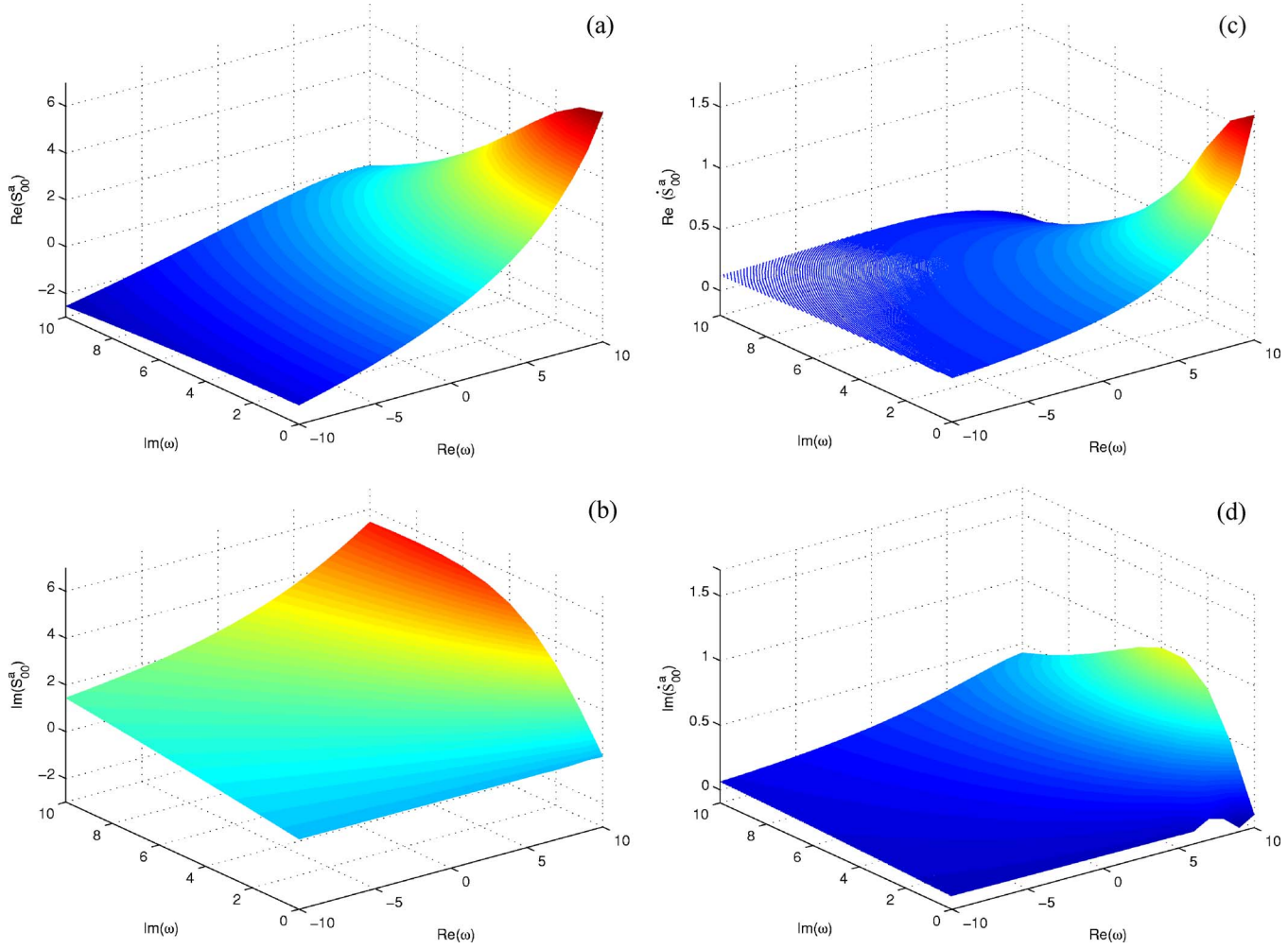

FIG. 1. (Color online) Real (a) and imaginary (b) parts of the *ss* element of the slope matrix $S^a_{0,0}(\omega)$, and real (c) and imaginary (d) parts of its first energy derivative $\dot{S}^a_{0,0}(\omega)$ calculated for the fcc structure (see text for further details).

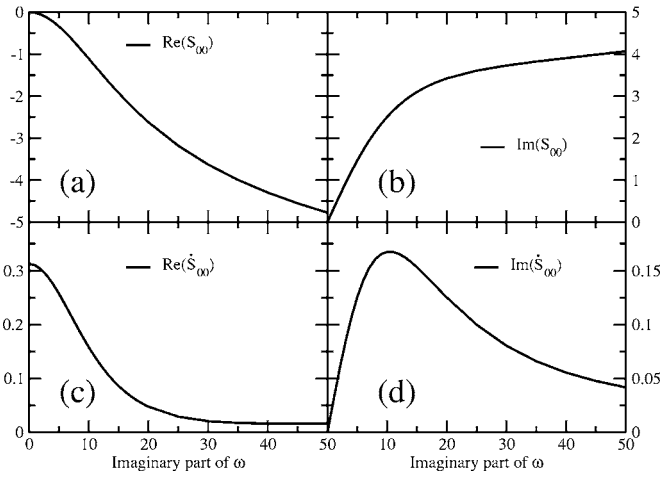

FIG. 2. Real (a) and imaginary (b) parts of the *ss* element of the slope matrix $S^a_{0,0}(\omega)$, and real (c) and imaginary (d) parts of its first energy derivative $\dot{S}^a_{0,0}(\omega)$ calculated for the fcc structure as functions of the imaginary values of (ω).

B. Expansion of the slope matrix

We establish the accuracy of the proposed one-center and two-center expansions of the slope matrix, by calculating the relative error of the expansions within the complex plane. We define the relative error as

$$\mathrm{Err} = \frac{\{[\mathrm{Re}(S_{\mathrm{calc}} - S_{\mathrm{expan}})]^2 + [\mathrm{Im}(S_{\mathrm{calc}} - S_{\mathrm{expan}})]^2\}^{1/2}}{\{[\mathrm{Re}(S_{\mathrm{calc}})]^2 + [\mathrm{Im}(S_{\mathrm{calc}})]^2\}^{1/2}}, \qquad (17)$$

where S_{calc} and S_{expan} are the *ss* elements of the calculated and estimated slope matrices or their first energy derivatives. This quantity is plotted in Fig. 3 as a function of energy for the case of the one-center expansion (13) with $\omega_0=(0,0)$. Panels (a) and (b) show Err for the slope matrix and its first derivative calculated using six and five derivatives. In panels (c) and (d) we give the same quantities obtained using three and two derivatives, respectively. Obviously, the sixth order expansion is superior compared to the third order expansion, but it is difficult to state explicitly for which values of ω the expansion breaks down. There is a gradually increasing error and whether the expansion works or not depends on the accuracy needed. The sixth order expansion reproduces the cal-

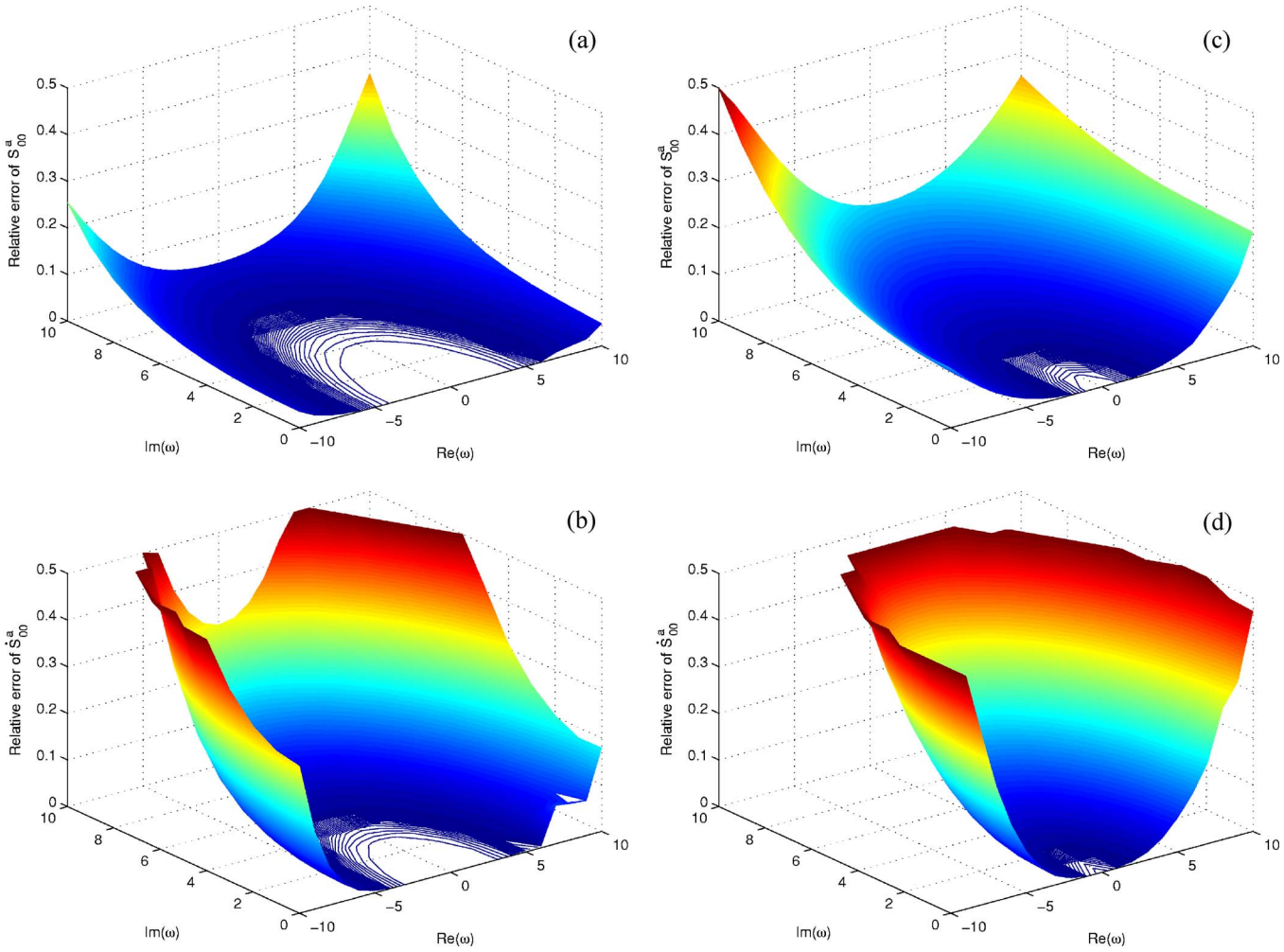

FIG. 3. (Color online) Relative error of the expansion (13) for (a) the slope matrix using six derivatives, (b) its first energy derivative using five derivatives, (c) the slope matrix using three derivatives, and (d) its first energy derivative using two derivatives. The error is defined in Eq. (17) and the expansion center is $\omega_0=(0,0)$. Values over 0.5 have been removed for clarity.

culated values S_{calc} with an accuracy better than $\sim 1\%$ within a radius of ~ 5 around the expansion center [Fig. 3(a)]. For a radius of ~ 10, the error of the expansion still is below 5%. However, around $\omega=(-10,10)$ the relative error reaches one third of S_{calc}. The situation is much worse in the case of the first order energy derivative [Fig. 3(b)]. Here, the relative error remains below a few percent for $|\omega| \lesssim 5$, but it increases to $\sim 30\%$ for $|\omega|=10$ and to $\sim 250\%$ around $(-10,10)$. The expansion can not be improved significantly by choosing the expansion center out in the complex plane. This is illustrated in Fig. 4, where the expansion center was set at $\omega_0=(3,3)$ instead of (0, 0) used for Fig. 3. As one can see, the convergence of the expansion is roughly the same as the one observed in the case of real ω_0.

The two-center expansion (14) is demonstrated in Fig. 5. The two expansion centers were set in $\omega_1=(0,0)$ and $\omega_2=(-10,0)$, and the expansion was carried out to $n=m=6$. The small error near (0, 0) on panel (a) is due to the fact that the *ss* element of the fcc structure constant passes through zero near this point. The first thing we can observe from this figure is that the relative error remains below $\sim 1\%$ for the slope matrix [panel (a)] and below $\sim 2\%$ for its energy derivative [panel (b)] within a radius of $|\omega| \approx 10$ around $\sim(-8,0)$. What is interesting is that the two-center form not only improves S_{expan} for points near the expansion centers, but dramatically improves S_{expan} for points at the other end of the energy mesh, as well as out in the complex plane. In fact, it has turned out that using a two-center expansion with $n \approx m \approx 6$, for an average $w^2 \approx 10$ Bohr^2 one can accurately map an energy window as large as ~ 0.5 Ry above and, depending on ω_2, 2–6 Ry below the Fermi level.

From the above results, we conclude that a Taylor expansion around real energies can be used to compute with high accuracy the elements of the slope matrix for an arbitrary complex energy. Furthermore, the two-center expansion seems to offer a way to improve on the one-center expansion in the case of wide bands.

C. A case in point: hcp La

Early transition metals are typical systems which have large characteristic bandwidth at ambient pressure. In these elements, the semicore states are located with $\sim 1-2$ Ry below the bottom of the valence band. In most cases, these

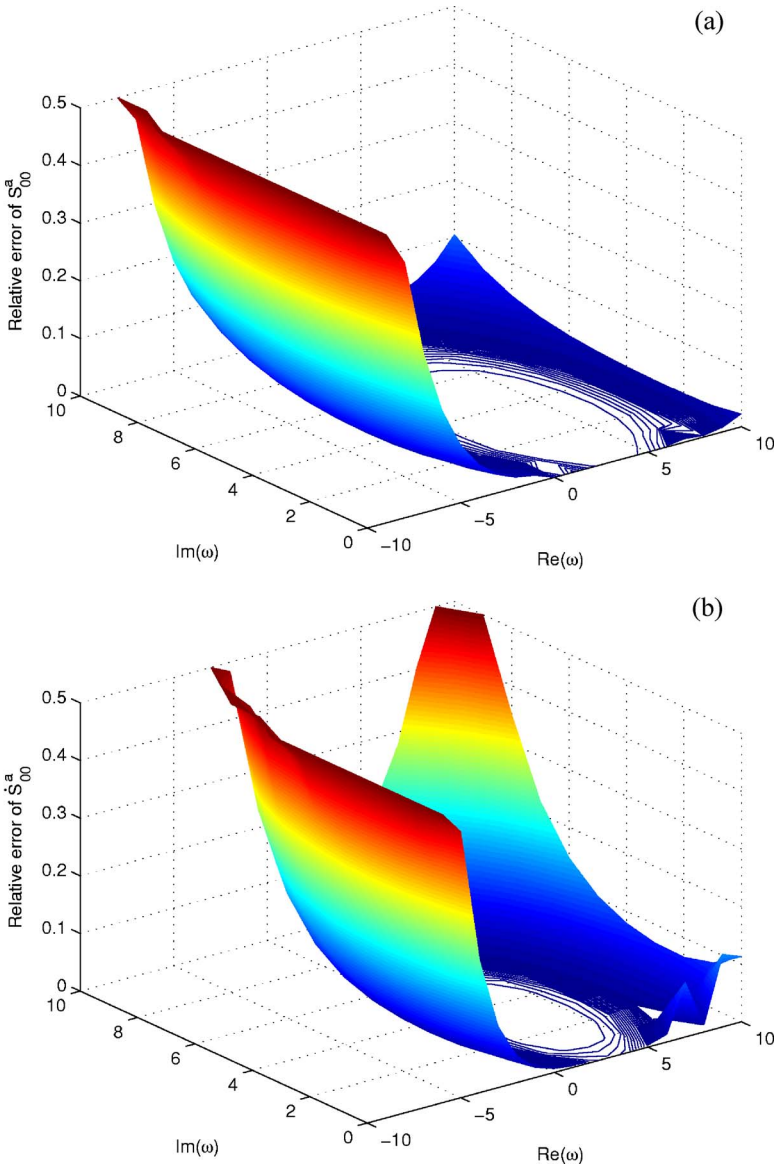

FIG. 4. (Color online) Relative error of the one-center expansion (13) for (a) the slope matrix using six derivatives and (b) its first energy derivative using five derivatives. The expansion center is $\omega_0=(3,3)$. Values over 0.5 have been removed for clarity.

states must be included in the self-consistent calculations directly rather than being frozen in the core or treated as atomiclike soft-core states. As an example, we consider the hexagonal close packed (hcp) La.

We illustrate the problem that may show up in connection with a large bandwidth by calculating the total energy of hcp La as a function of volume using different parametrizations for the slope matrix. In this test, we adopted the generalized gradient approximation[49] (GGA) for the exchange-correlation functional. The density of states for hcp La calculated at the experimental volume, is plotted in Fig. 6 as a function of energy with respect to the Fermi level. The $5p$ semicore states of La can be seen as the peaks in the density of states around −1.2 Ry. Therefore, in order to treat the semicore states on equal footing with the valence states, the contour used for the energy integration must be expanded from 0 down to approximately −1.5 Ry. We note that putting the $5p$ states in the core and thereby making it possible to use a small energy contour, fails completely in getting a reasonable equation of state for hcp La.

Using the experimental atomic radius of double-hcp La,[50,51] the above energy window for La corresponds to $-16\lesssim\omega\lesssim 7$ (see the upper horizontal axis in Fig. 6) in units of the dimensionless parameter $\omega=(\epsilon-v_0)w^2$. Hence, the slope matrix has to be parametrized either with more than one one-center expansion (13) or with the two-center expansion (14). If we opt for two one-center expansions, we need to use two different ω_0 values, one set around the muffin-tin zero and another close to the semicore states. In this case, special attention must be paid when choosing the energy contour in order to avoid the errors coming from energies joining the two analytic expressions. The usual circular energy contour can lead to oscillations in the total energy, as illustrated by the dashed line from Fig. 7. We can get rid of this unphysical oscillations by dividing the original circular contour into two small contours, one energy window enclosing the valence states ($-0.5\lesssim\epsilon\lesssim 0$) and the other the semicore states ($-1.5\lesssim\epsilon\lesssim -1.0$). On the other hand, the two-center expansion is expected to offer a more elegant solution to the above problem. Indeed, as it can be seen in Fig. 7

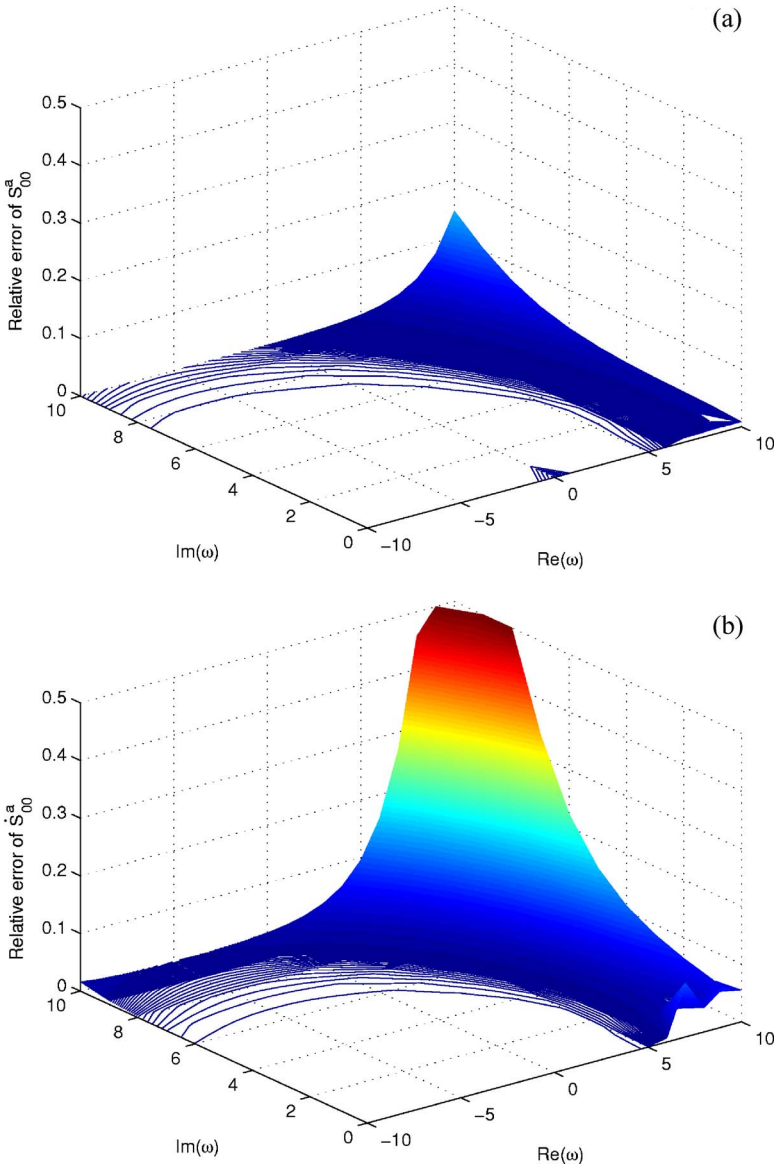

FIG. 5. (Color online) Relative error of the expansion of (a) the slope matrix and (b) its first energy derivative using the two-center expansion (14). The two expansion centers are $\omega_1=(0,0)$ and $\omega_2=(-10,0)$. Values over 0.5 have been removed for clarity.

(solid line), the two-center expansion (14) produces a smooth energy versus atomic radius curve.

In a self-consistent calculation, the electron count is realized via the overlap matrix, and thus via the energy derivative of the slope matrix.[47] On the other hand, in the FCD formalism,[26] the total number of electrons is found directly by integrating the electron density within the unit cell. In an ideal situation, this integral should give exactly the total number of electrons. However, in practice there is always a charge misfit Δ_e. When all the numerical parameters controlling the real space integration are set to their converged values, the requirement $\Delta_e \rightarrow 0$ is one of the most severe test for the accuracy of the slope matrix and its energy derivative. Using two one-center expansions, we obtain $\Delta_e=0.0108$ for hcp La near the equilibrium volume. At the same time, this figure decreases to 0.0006 when the two-center expansion (14) is employed. This clearly demonstrates the superiority of Eq. (14) compared to Eq. (13) in the case of systems with large bandwidth.

IV. COMPOSITIONAL DISORDER IN MgY THIN FILMS

In systems containing elements with semicore states, even when the one-center expansion works reasonably well for the pure elements, the effect of alloying may lead to the semicore states hybridizing with the valence states and thus creating large errors in the calculations. In contrast to the one-center expansion, the proposed two-center expansion can be applied to such systems as well. Here we illustrate this in the case of hcp MgY alloys.

Hydrogen storage is an important research area, since materials, which can both store hydrogen and later release it, are imperative for the future fuel cell techniques. Magnesium is a material with very high hydrogen uptake.[52] Unfortunately, pure Mg has thermodynamic and kinetic limitations,[53] which may be overtaken by alloying. In a recent paper,[54] it was suggested that one could use Y, since Y hydrides form very easily. In bulk samples, the solubility limit of Y in Mg is less than 1% at room temperature and ~4% at 800 K.[55] Surprisingly, in samples obtained by sputtering Mg and Y onto a

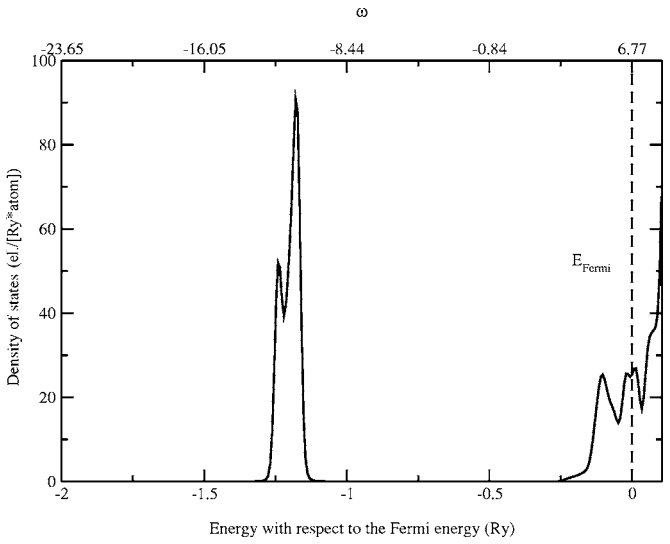

FIG. 6. Calculated density of states for hcp La. The 5*p* semicore states are located around an energy of −1.2 Ry. The energy in the bottom axis is shown in Ry (relative to the Fermi energy). The upper horizontal axis shows it in units of ω.

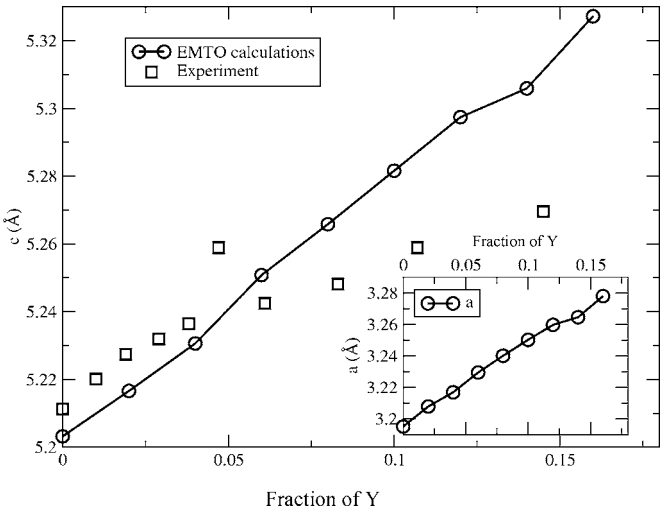

FIG. 8. Calculated (circles) and experimental (squares) values of the hexagonal lattice parameter c for the hcp $Mg_{1-x}Y_x$ alloy as a function of x. The experimental values are taken from Ref. 54. The inset shows the theoretical prediction of the concentration dependence of the lattice parameter a for the same system.

glass substrate,[54] measurements indicated the possibility to obtain an hcp solid solution between Mg and Y up to an Y concentration of 17%. The lattice parameter c of this hcp Mg-Y system was measured as a function of alloy composition. Here, we calculate the concentration variation of the lattice parameters of Mg-Y as function of Y content and compare the obtained hexagonal lattice parameter with the above mentioned experimental data.

The calculations were carried out using the EMTO method, which has been proven to be accurate enough for the optimization of the c/a ratio in random alloys.[33,38] Since Y has semicore states, for the slope matrix we used the suggested two-center Taylor expansion in order to assure a good description of the energy dependence. This is especially important since we had to minimize the total energy with respect to c/a ratio for the hcp lattice. In the basis set we included s,p,d,f orbitals, and the k-space sampling was done using $1573k$ points in the irreducible part of the Brillouin zone. For the exchange correlation we used GGA functional.[49]

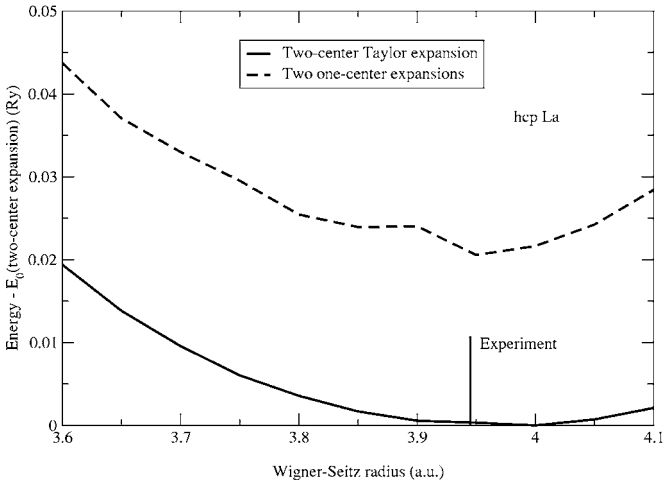

FIG. 7. Equation of state for hcp La, calculated using a two-center expansion (solid line) or two one-center expansions (dashed line) for the energy dependence of the slope matrix. The vertical line indicates the experimental Wigner-Seitz radius for dhcp La taken from Ref. 51.

The calculated lattice parameter c is plotted in Fig. 8 together with the experimental values from Ref. 54. The theoretical prediction for the a lattice parameter is also shown (inset). We note that for pure Mg the calculated values of the lattice parameters a and c, 3.19 and 5.20 Å, respectively, are in excellent agreement with the experimental values of $a=3.21$ Å and $c=5.21$ Å.[51,54] As it can be seen, the slope of the calculated concentration dependence of the lattice parameter c agrees with the slope of the experimental curve very well up to ~4% Y. At higher Y concentrations, a new branch seems to appear at the experimental curve, with a substantially different slope. On the other hand, our calculations show that for random Mg-Y alloys with high Y content, c follows the same curve as for diluted alloys, with a constant slope. As a matter of fact, this should be expected if the alloy stays in a single solid solution phase. Our theoretical value for Y, $a=3.68$ Å and $c=5.81$ Å, are slightly higher than the experimental values $a=3.65$ Å and $c=5.73$ Å.[51]. However, an extrapolation of the experimental branch above ~5% Y towards pure Y leads to an estimate of the lattice parameter c around 5.4 Å. This is much lower than the experimental value for pure Y, mentioned above. Thus, the increasing difference between the theoretical and experimental curves at high Y concentration could indicate that the experimental films are no longer in a single solid solution phase, and may contain some precipitates of the second phase. Perhaps further investigation of the alloy would be of interest.

Finally, we would like to note that our test calculations, performed by considering the semicore states of Y as a part of the core and thus using one-center expansion for the slope

matrix, gave results in worse agreement with experiment than those from Fig 8. For instance, at 4% Y, for c we obtained 5.219 Å using the one-center expansion, which should be compared to 5.231 Å obtained using the two-center form or 5.235 Å reported in experiment. This is of course to be expected both with regards to the sensitivity of the c/a minimization, the problem with the hybridizing semicore states of Y, and the increase in accuracy in general due the two-center expansion.

V. CONCLUSIONS

We have investigated the behavior of the EMTO slope matrix and its first energy derivative in the complex energy plane. We have shown that although the bare structure constants decay exponentially for large imaginary parts of the energy, the screening introduces another energy dependence of the slope matrix. This is calculated numerically and analytical formulae for the energy dependence in this energy region are derived. We have found that for large imaginary energies, the diagonal elements of the EMTO slope matrix converge towards $(i\sqrt{\omega}-1)$.

We have investigated the accuracy of the one-center and two-center expansions for the energy dependence of the slope matrix and its first energy derivative. We have found that one can safely use the Taylor expansion from the real axis, provided that one uses enough terms in the expansion and not expand too far from the expansion center/centers. We have demonstrated that the two-center expansion works well for a larger energy window and can be used to describe systems with large bandwidth. Furthermore, there are cases, here exemplified by hcp La, where special care must be paid when using separate expansions for the valence and semicore states. The two-center expansion is found to offer a more elegant and more accurate solution to treat such systems.

We also investigated the Mg rich Mg-Y alloys, which is a material of interest for hydrogen storage applications. Calculations agree well with experimental values for Y concentration below ~4% and show that in thin films a single phase solid solution is probably stable only up to 4–5% of Y in hcp Mg.

ACKNOWLEDGMENTS

This work was supported by the Swedish Research Council, the Swedish Foundation for Strategic Research and the research project OTKA Grants No. T046773 and No. T048827 of the Hungarian Scientific Research Fund. Most of the calculations were carried out at the National Supercomputer Center in Linköping, Sweden. I.A.A. thanks B. Hjörvarsson and M. Persson for useful discussions and help with this project and L.V. thanks J. Kollár for discussions.

[1] V. Heine, *Solid State Physics*, edited by H. Ehrenreich, F. Seitz, and D. Turnbull (Academic, New York, 1970), p. 1.
[2] W. A. Harrison, *Pseudopotentials in the Theory of Solids* (Bejamin, New York, 1966).
[3] M. L. Cohen and V. Heine, *Solid State Physics*, edited by H. Ehrenreich, F. Seitz, and D. Turnbull (Academic, New York, 1970), p. 37.
[4] J. Korringa, Physica (Utrecht) **13**, 392 (1947).
[5] W. Kohn and J. Rostoker, Phys. Rev. **94**, 1111 (1954).
[6] O. K. Andersen, Solid State Commun. **13**, 133 (1973).
[7] O. K. Andersen and R. G. Wolley, Mol. Phys. **26**, 905 (1973).
[8] O. K. Andersen, Phys. Rev. B **12**, 3060 (1975).
[9] A. R. Williams, J. Kübler, and C. D. Gelatt, Jr., Phys. Rev. B **19**, 6094 (1979).
[10] H. L. Skriver, *The LMTO Method* (Springer, New York, 1984).
[11] O. K. Andersen, A. V. Postnikov, and S. Y. Savrasov, *The Muffin-Tin-Orbital Point of View*, MRS Symp. Proc. No. 253 (Materials Research Society, Pittsburgh, 1992), pp. 37–70.
[12] O. K. Andersen (unpublished).
[13] O. K. Andersen and O. Jepsen, Phys. Rev. Lett. **53**, 2571 (1984).
[14] I. A. Abrikosov, A. M. N. Niklasson, S. I. Simak, B. Johansson, A. V. Ruban, and H. L. Skriver, Phys. Rev. Lett. **76**, 4203 (1996).
[15] I. A. Abrikosov, S. I. Simak, B. Johansson, A. V. Ruban, and H. L. Skriver, Phys. Rev. B **56**, 9319 (1997).
[16] W. R. Lambrecht and O. K. Andersen, Surf. Sci. **178**, 256 (1986).
[17] H. L. Skriver and N. M. Rosengaard, Phys. Rev. B **43**, 9538 (1991).
[18] R. Zeller, P. H. Dederichs, B. Ujfalussy, L. Szunyogh, and P. Weinberger, Phys. Rev. B **52**, 8807 (1995).
[19] K. Wildberger, R. Zeller, and P. H. Dederichs, Phys. Rev. B **55**, 10074 (1997).
[20] D. M. C. Nicholson, G. M. Stocks, Y. Wang, W. A. Shelton, Z. Szotek, and W. M. Temmerman, Phys. Rev. B **50**, 14686 (1994).
[21] Y. Wang, G. M. Stocks, W. A. Shelton, D. M. C. Nicholson, Z. Szotek, and W. M. Temmerman, Phys. Rev. Lett. **75**, 2867 (1995).
[22] O. K. Andersen, O. Jepsen, and G. Krier, *Lectures on Methods of Electronic Structure Calculations* (World Scientific Publishing, Singapore, 1994), pp. 63–124.
[23] L. Vitos, Phys. Rev. B **64**, 014107 (2001).
[24] L. Vitos, in *Recent Research Developments in Physics* (Transworld Research Network Publisher, Trivandrum, India, 2004), Vol. 5, pp. 103–140.
[25] L. Vitos, H. L. Skriver, B. Johansson, and J. Kollár, Comput. Mater. Sci. **18**, 24 (2000).
[26] J. Kollár, L. Vitos, and H. L. Skriver, *Electronic Structure and Physical Properties of Solids: The Uses of the LMTO Method*, edited by H. Dreyssé, Lecture Notes in Physics (Springer-Verlag, Berlin, 2000), pp. 85–113.
[27] L. Vitos, B. Johansson, J. Kollár, and H. L. Skriver, Phys. Rev. B **62**, 10046 (2000).
[28] L. Vitos, B. Johansson, and J. Kollár, Phys. Rev. B **62**, R11957 (2000).
[29] B. Magyari-Köpe, L. Vitos, and J. Kollár, Phys. Rev. B **63**, 104111 (2001).
[30] B. Magyari-Köpe, L. Vitos, B. Johansson, and J. Kollár, Acta Crystallogr., Sect. B: Struct. Sci. **57**, 491 (2001).

[31] P. Soven, Phys. Rev. **156**, 809 (1967).
[32] B. L. Györffy, Phys. Rev. B **5**, 2382 (1972).
[33] L. Vitos, I. A. Abrikosov, and B. Johansson, Phys. Rev. Lett. **87**, 156401 (2001).
[34] L. Vitos, P. A. Korzhavyi, and B. Johansson, Nat. Mater. **2**, 25 (2003).
[35] P. Olsson, I. A. Abrikosov, L. Vitos, and J. Wallenius, J. Nucl. Mater. **321**, 84 (2003).
[36] L. Vitos, P. A. Korzhavyi, and B. Johansson, Phys. Rev. Lett. **88**, 155501 (2002).
[37] B. Magyari-Köpe, G. Grimvall, and L. Vitos, Phys. Rev. B **66**, 064210 (2002).
[38] B. Magyari-Köpe, L. Vitos, and G. Grimvall, Phys. Rev. B **70**, 052102(4), (2004).
[39] A. E. Kissavos, S. I. Simak, P. Olsson, L. Vitos, and I. A. Abrikosov, Comput. Mater. Sci. **35**, 1 (2006).
[40] R. Zeller, J. Deutz, and P. H. Dederichs, Solid State Commun. **44**, 993 (1982).
[41] V. I. Anisimov, A. I. Poteryaev, M. A. Korotin, A. O. Anokhin, and G. Kotliar, J. Phys.: Condens. Matter **9**, 7359 (1997).
[42] A. I. Lichtenstein and M. I. Katsnelson, Phys. Rev. B **57**, 6884 (1998).
[43] L. Chioncel, L. Vitos, I. A. Abrikosov, J. Kollár, M. I. Katsnelson, and A. I. Lichtenstein, Phys. Rev. B **67**, 235106 (2003).
[44] A. I. Lichtenstein (private communication).
[45] O. K. Andersen and C. Arcangeli (unpublished).
[46] M. Abramowitz and I. A. Stegun, *Handbook of Mathematical Functions* (Dover, New York, 1970).
[47] L. Vitos (unpublished).
[48] O. K. Andersen, O. Jepsen, and M. Sob, *Electronic Band Structure and its Applications*, edited by M. Yussouff (Springer-Verlag, Berlin, 1987).
[49] J. P. Perdew, K. Burke, and M. Ernzerhof, Phys. Rev. Lett. **77**, 3865 (1996).
[50] D. A. Young, *Phase Diagrams of the Elements* (University of California Press, Berkeley, 1991).
[51] C. Kittel, *Introduction to Solid State Physics*, 7th ed. (Wiley, New York, 1996).
[52] K. C. Hoffman, J. J. Reilly, F. J. Salzano, C. W. Waide, R. H. Wiswall, and W. E. Winsche, Int. J. Hydrogen Energy **1**, 133 (1976).
[53] J. F. Stampfer, Jr., C. E. Holley, Jr., and J. F. Suttle, J. Am. Chem. Soc. **82**, 3505 (1960).
[54] C. Chacon, E. Johansson, B. Hjörvarson, C. Zloeta, and Y. Andersson, J. Appl. Phys. **97**, 104903 (2005).
[55] T. B. Massalski, *Binary Alloy Phase Diagrams* (ASM International, Metals Park, OH, 1990).